Model and Control of a Six-Pole Magnetic Bearing

Laura Julia Martins Mothé[1], Vinícius Ramos Vasco[2], Yago Pessanha Corrêa[3], Domingos de Farias Brito David[4], and Afonso Celso Del Nero Gomes[5]

[1] Universidade Federal do Rio de Janeiro (UFRJ)
lauramothe@gmail.com
[2] Marinha do Brasil (*Brazilian Navy*)
viniciusramosvasco@gmail.com
[3] Instituto Federal Fluminense (IFFluminense)
yago.correa@iff.edu.br
[4] Universidade Federal Fluminense (UFF)
domingos@vm.uff.br
[5] Universidade Federal do Rio de Janeiro (UFRJ)
nero@coep.ufrj.br

Abstract

Mechanical Bearings are machine elements that support the rotating axes and promote smooth movement between contact surfaces. In order to eliminate friction between the parts and, consequently, the need for lubrication, Active Magnetic Bearings (AMB) were developed based on the generation of reluctance electromagnetic forces. Due to the unstable nature of this equipment, it is necessary to implement a control strategy to avoid displacements and keep the axis aligned. There are studies about different geometries of magnetic bearings regarding the number of poles they present. The eight and four-pole configurations are the most usual, although other alternatives are being studied, like the three and six-pole geometry. The main objective of this paper is to present a mathematical model for the six-pole magnetic bearing applied to a vertical rotor system, propose control strategies to stabilize the system and compare its performance to the four and eight-pole bearings. In addition, comparisons between rotational speeds are carried out to define low, medium and high rotational ranges, and a study on the system's response to control designed for a certain rotational speed in the system operating at different speeds.

1 Background

Bearings are mechanical transmission elements designed to support loads applied to a rotating shaft, promoting movement between the contact surfaces by reducing friction between them. They keep the axis aligned, preventing perpendicular displacements. Since the bearing is a fixed component in contact with another that moves, the friction generated results in a loss of efficiency in the transference of mechanical energy. In order to reduce this loss and increase the operating life of the bearings, lubrication is necessary periodically. However, the use of lubricating oils presents burdens such as time demands for maintenance, high costs, risks of environmental contamination and restrictions on use in some industrial sectors [1].

Alternatively, with the objective of mitigating the disadvantages mentioned with the application of conventional mechanical bearings, a new field of research has emerged and has become increasingly prominent: Magnetic Bearings. Based on the generation of restoring forces capable of preventing radial and axial movements of the rotating axis, its main characteristic is the absence of mechanical contact between the surfaces and, consequently, the elimination of friction [2]. The restorative forces that govern the operation of Magnetic Bearings are obtained through the injection of voltage or current in electromagnets strategically located radially to the axis.

To determine these input variables and keep the axis aligned, it is necessary to apply a control strategy, which leads to calling this devices Active Magnetic Bearings (AMBs).

There are some possible geometries for Magnetic Bearings in relation to the stator pole number. Currently, the three best known geometries are the eight, four and three-pole. These three geometries differ in heat dissipation, magnetic flux loss, interconnection of fluxes, and the reluctance force equations, which leads to different models for each one [3].

The main objective of this work, following the research area of Magnetic Bearings, is to develop and present a mathematical model for the six-pole magnetic bearing applied to a system with a vertical rotor and propose control strategies to stabilize the system. Furthermore, a comparative study between the six, four and eight-pole bearings performance is presented from simulations. Two other studies are also carried out: comparisons between rotational speeds to define low, medium and high rotational ranges, and the response to control laws designed for a specific rotational speed in the system operating at different speeds.

2 Discussion

At present, there are two AMBs configurations that are better known and applied: the most common and traditional, eight-pole configuration [4][5][6], and also the four-pole configuration [7][8]. It can be said that these two cases have symmetry of 4, since the reluctance forces applied to the rotor come from 4 points located on the canonical x (horizontal) and y (vertical) axes.

There are other possible topologies for AMBs, such as three [1][9], six and twelve-pole, however, they are found less frequently. These geometries have symmetry of 3, where the magnetic forces applied to the rotor come from 3 coplanar points, none of them in the canonical x, y directions, in general; one of these points, at most, can lie in either the x or the y directions.

This paper adresses the development of the reluctance forces and modelling the dynamic system in state space for the six-pole AMB which will be simulated in order to compare its performance with the eight and four-pole configuration.

In the six-pole AMBs, there are three channels with two poles each, spatially separated by $(2\pi/3)$rad angles. A basic illustration of this scheme is presented in Figure 1. The rotor shaft is to be positioned at the origin of an x, y canonical coordinate system. This position is controlled using the magnetic forces $\mathbf{F}_k(t)$ for $k = 1, 2, 3$, generated by electromagnetic principle from the injection of currents in each pair of poles of the stator.

The main influence on the magnetic forces is the square of the magnetic flux $\phi_k(t)$ [7], as shown in Equation 1:

$$F_k = \frac{\phi_k^2(t)}{2\mu_0 A} \quad \text{for} \quad k = 1, 2, 3, \tag{1}$$

where μ_0 is the magnetic permeability and A is the winding cross area through which the flux passes.

The three fluxes ϕ_k are said to be decoupled, since each one of them does not intercept the other two. All the flux injected in the rotor by one of the poles in channel k is absorbed by the other pole in the same channel.

Considering $d_k(t)$ for $k = 1, 2, 3$ the gap width at pole k, Equation 1 can be rewritten so that the magnitude of the reluctance force generated is [10]:

$$F_k = K\left(\frac{i_k(t)}{d_k(t)}\right)^2 \quad \text{with} \quad K = \frac{\mu_0 A n^2}{4} \quad \text{for} \quad k = 1, 2, 3, \tag{2}$$

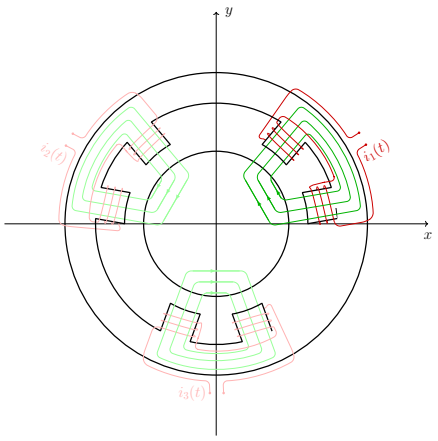

Figure 1: Six-pole configuration for Active Magnetic Bearings. Channel 1 is composed of the pair of poles above and to the right, making an angle of $(\pi/3)$rad with the x axis.

where i_k is the injected current and n is the number of coil windings. Therefore, the flux ϕ_k depends only on the current i_k and the distance d_k.

The spatial directions of the three magnetic forces generated in the six-pole AMB, projected in the x and y directions, lead to

$$F^x(t) = F_1(t)\cos\frac{\pi}{6} - F_2(t)\cos\frac{\pi}{6} + F_3(t)\cos\frac{3\pi}{2} \tag{3}$$

$$F^y(t) = F_1(t)\,\mathrm{sen}\,\frac{\pi}{6} + F_2(t)\,\mathrm{sen}\,\frac{\pi}{6} + F_3(t)\,\mathrm{sen}\,\frac{3\pi}{2}. \tag{4}$$

Applying Equation 2 into Equations 3 e 4, we obtain the resultant magnetic forces on the rotor. Omitting (t) in the time-varying signals, the resultants are:

$$F^x = \frac{K\sqrt{3}}{2}\left[\left(\frac{i_1}{d_1}\right)^2 - \left(\frac{i_2}{d_2}\right)^2\right] \tag{5}$$

$$F^y = \frac{K}{2}\left[\left(\frac{i_1}{d_1}\right)^2 + \left(\frac{i_2}{d_2}\right)^2 - 2\left(\frac{i_3}{d_3}\right)^2\right]. \tag{6}$$

The rotor's distances to the poles $d_k(t)$ can be denoted by Equation 7, where h is the nominal gap width and e_k measure the rotor's displacement from the origin in the direction of pole k.

$$d_k(t) = h - e_k(t) \quad \text{for} \quad k = 1, 2, 3. \tag{7}$$

It can be seen that the e_k displacements are redundant to determine the rotor's position in the plane and only two values are sufficient for this purpose. Projecting the displacements on the canonical directions x and y leads to:

$$e_1(t) = x(t)\cos\frac{\pi}{6} + y(t)\,\mathrm{sen}\,\frac{\pi}{6} \tag{8}$$

$$e_2(t) = -x(t)\cos\frac{\pi}{6} + y(t)\,\mathrm{sen}\,\frac{\pi}{6} \tag{9}$$

$$e_3(t) = x(t)\cos\frac{3\pi}{2} + y(t)\,\text{sen}\,\frac{3\pi}{2} = -y(t). \tag{10}$$

Applying equations 7, 8, 9 e 10 to the reluctance forces equations 5 and 6 and linearizing around the operating point $OP = (i_1^0, i_2^0, i_3^0, x^0, y^0) = (0, 0, 0, 0, 0)$ leads to an uncontrollable model. To solve this problem, it is possible to apply the base and differential currents concept: $i_k(t) = i_0 + v_k(t)$ for $k = 1, 2, 3$, where i_0 is a fixed base current and v_k are differential currents.

At first, it is reasonable to consider a particular case where the 3 currents v_k can be expressed in terms of only 2 differential currents i_x and i_y:

$$i_1(t) = i_0 + i_x(t) + i_y(t) \tag{11}$$

$$i_2(t) = i_0 - i_x(t) + i_y(t) \tag{12}$$

$$i_3(t) = i_0 - i_y(t). \tag{13}$$

Combining Equations 5 to 13, we can obtain a complete mathematical model for the reluctance forces generated in the 6-pole AMB. The linearization of this model around the operating point $O = (i_x^0, i_y^0, x^0, y^0) = (0, 0, 0, 0)$ results in:

$$F^x(t) = k_p x(t) + 2\sqrt{3}k_v i_x(t) \tag{14}$$

$$F^y(t) = k_p y(t) + 4k_v i_y(t) \tag{15}$$

$$k_p = 3\frac{\mu_0 A n^2 i_0^2}{4h^3} \qquad \text{and} \qquad k_v = \frac{\mu_0 A n^2 i_0}{4h^2}. \tag{16}$$

The model presents decoupled structure, which is a desirable fact and will make the control of 6 poles AMBs easier.To further understand how these magnetic forces interact with the x and y displacements of the rotor, a dynamic mathematical model is necessary.

In the Magnetic Bearing, the stator is responsible for generating the magnetic forces while all dynamic aspects depend on the shaft. For this work, it will be considered a rigid and homogeneous rotor in the vertical position. Center of mass displacements can be determined by the angles α and β. The dynamics of the shaft is described by

$$J\ddot{\boldsymbol{p}}(t) + G\dot{\boldsymbol{p}}(t) = \boldsymbol{E}(t), \tag{17}$$

where J is the inertia coefficient (or inertia matrix JI_2), $\boldsymbol{p} = \begin{bmatrix}\beta & -\alpha\end{bmatrix}$ is the position vector based on the angular movements of the shaft, G is the gyroscopic matrix:

$$G = \begin{bmatrix} 0 & \omega I_z \\ -\omega I_z & 0 \end{bmatrix} = \omega I_z \begin{bmatrix} 0 & 1 \\ -1 & 0 \end{bmatrix}, \tag{18}$$

which depends on the rotation speed ω, and $\boldsymbol{E}$ is the external excitation vector. Three external excitations are considered: magnetic, gravitational and supporting bearing [7].

From Equation 17, as can be seen in [7], it is possible to obtain the state space system model, shown in equation 19 allowing the application of modern control techniques:

$$\dot{\boldsymbol{x}}(t) = A\boldsymbol{x}(t) + B\boldsymbol{v}(t), \tag{19}$$

where A and B are, respectively, 4×4 and 4×3 matrices structured as follows:

$$A = \begin{bmatrix} 0_2 & I_2 \\ A_{21} & A_{22} \end{bmatrix} \qquad B = \begin{bmatrix} B_1 \\ B_2 \end{bmatrix}, \tag{20}$$

in which

$$A_{21} = J^{-1}b^2k_pI_2 = A_{21}(k_p) \qquad A_{22} = -J^{-1}(G + C_a) = A_{22}(\omega) \tag{21}$$

$$B_1 = 0_{2\times3} \qquad B_2 = J^{-1}bdk_vV = B_2(k_v), \tag{22}$$

where I is an identity matrix, the other variables are constructive parameters of the prototype and the state variables vector $\boldsymbol{x}$ is chosen to be

$$\boldsymbol{x} = \begin{bmatrix} x_s \\ y_s \\ \dot{x}_s \\ \dot{y}_s \end{bmatrix}. \tag{23}$$

Since the injected currents i_k are the control variables of the system, the control vector $\boldsymbol{v}$ is defined considering equations 11, 12 and 13

$$\boldsymbol{v}(t) = \begin{bmatrix} v_1(t) \\ v_2(t) \\ v_3(t) \end{bmatrix} = \begin{bmatrix} i_x(t) + i_y(t) \\ -i_x(t) + i_y(t) \\ -i_y(t) \end{bmatrix} = \begin{bmatrix} 1 & 1 \\ -1 & 1 \\ 0 & -1 \end{bmatrix} \begin{bmatrix} i_x(t) \\ i_y(t) \end{bmatrix}. \tag{24}$$

Making the vector $[i_x(t) \;\; i_y(t)]^T = \boldsymbol{u}(t)$, equation 19 can be rewritten into a structure with only two control variables, the differential currents $i_x(t)$ and $i_y(t)$

$$\dot{\boldsymbol{x}}(t) = A\boldsymbol{x}(t) + B^d\boldsymbol{u}(t), \qquad \text{where } B^d = \frac{bdk_v}{J} \begin{bmatrix} 0 & 0 \\ 0 & 0 \\ 2\sqrt{3} & 0 \\ 0 & 4 \end{bmatrix}. \tag{25}$$

The output vector is formed by the signals measured by sensors $x_s(t)$ and $y_s(t)$.

$$\boldsymbol{z}(t) = \begin{bmatrix} x_s(t) \\ y_s(t) \end{bmatrix} = \begin{bmatrix} 1 & 0 & 0 & 0 \\ 0 & 1 & 0 & 0 \end{bmatrix} \dot{\boldsymbol{x}}(t) = C\dot{\boldsymbol{x}}(t) \tag{26}$$

In order to keep the shaft centralized, an active control strategy is needed to find an input capable of stabilizing the system. This paper addresses the optimal control based on the Linear Quadratic Regulator (LQR) theory, considering two types of schemes: centralized and decentralized.

The block diagram in Figure 2 represents the closed-loop system achieved for the six-pole AMB. In this case, the objective of the system is to reach the zero state to stabilize the rotor at the center of the coordinate system.

As shown in the block diagram, the control signal is defined by $\boldsymbol{u} = F\boldsymbol{x}$, since the reference value $\boldsymbol{r} = 0$. Therefore, the state equation can be rewritten as:

$$\dot{\boldsymbol{x}} = A\boldsymbol{x} + B^dF\boldsymbol{x} \tag{27}$$

where F is the feedback gain matrix, responsible for changing the system's closed-loop poles, once the system is controllable.

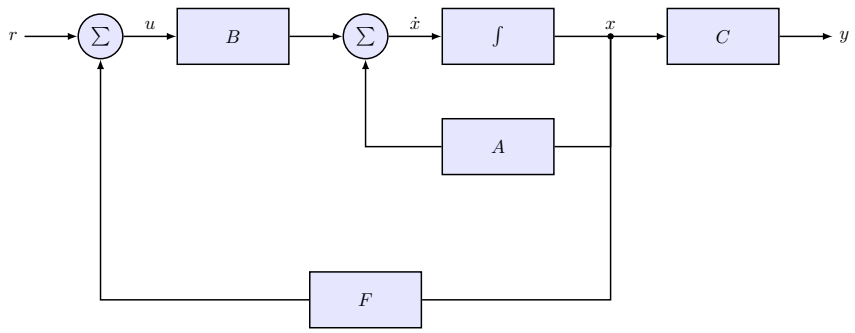

Figure 2: Full state feedback block diagram.

The LQR method has the advantage of providing a systematic model for calculating the gain matrix F [11]. The quadratic functional J expressed in equation 28 describes the index to be minimized:

$$J = \int_0^\infty (\boldsymbol{x}^T(t)Q\boldsymbol{x}(t) + \boldsymbol{u}^T(t)R\boldsymbol{u}(t))\ dt \tag{28}$$

where Q is a symmetric positive semidefinite matrix and R is a symmetric positive definite matrix, which detemine the state error and the energy consumption, respectively.

Considering that this is a controllable system with all states observable and available, the control law that minimizes J can be written:

$$\boldsymbol{u}^* = F^*\boldsymbol{x}. \tag{29}$$

Matrix F^* is given by:

$$F^* = -R^{-1}B_d^T P, \tag{30}$$

where P is the solution of an algebraic Riccati equation:

$$A^T P + PA - PBR^{-1}B_d^T P + Q = 0. \tag{31}$$

The optimal performance index of J is given by:

$$J = \boldsymbol{x}_\mathbf{0}^T P \boldsymbol{x}_\mathbf{0}, \tag{32}$$

where $\boldsymbol{x}_\mathbf{0}$ represents the initial state.

The LQR control technique just introduced is sometimes called centralized LQR (LQRc). In this case, when performing state feedback, each component of the control vector $\boldsymbol{u}$ depends on all state variables [10], as shown in Equation 33:

$$\boldsymbol{u} = F_c^*\boldsymbol{x} \implies \begin{bmatrix} u_1 \\ u_2 \end{bmatrix} = \begin{bmatrix} f_{11} & f_{12} & f_{13} & f_{14} \\ f_{21} & f_{22} & f_{23} & f_{24} \end{bmatrix} \begin{bmatrix} x_s \\ y_s \\ \dot{x}_s \\ \dot{y}_s \end{bmatrix}. \tag{33}$$

Therefore, it is expected that the feedback matrix F_c^* to have all nonzero elements, but this fact requires greater computational effort.

To overcome this inconvenience, decentralized LQR (LQRd) control can be implemented. The presence of null elements in the state feedback matrix prevents interactions between different states in the control application. These elements are located strategically so that the system has a decoupled behavior, that is, each of the two control variables is independent of the other, as shown in 34:

$$u_1 = f_{11}x_s + f_{13}\dot{x}_s \qquad \text{and} \qquad u_2 = f_{22}y_s + f_{24}\dot{y}_s. \tag{34}$$

Thus, the decentralized feedback gain matrix F_d^* assumes the following structure:

$$\begin{bmatrix} u_1 \\ u_2 \end{bmatrix} = \begin{bmatrix} f_{11} & 0 & f_{13} & 0 \\ 0 & f_{22} & 0 & f_{24} \end{bmatrix} \begin{bmatrix} x_s \\ y_s \\ \dot{x}_s \\ \dot{y}_s \end{bmatrix} = F_d^* \boldsymbol{x}. \tag{35}$$

Since each control variable is only related to one state variable, the state space vector $\boldsymbol{x}$ can be subdivided in two. Further details can be found in [10]. Thus, equation 35 can be rewritten so that the structure of the decentralized proposal is:

$$\boldsymbol{u} = \begin{bmatrix} p_1 & 0 & d_1 & 0 \\ 0 & p_2 & 0 & d_2 \end{bmatrix} \boldsymbol{x} = F_d^* \boldsymbol{x}, \tag{36}$$

where the notation used in the gain matrix refers to the PD (proportional-derivative) control laws, since each control variable relates only to one output and its derivative.

Equations 37 to 39 present the necessary conditions for F to satisfy 36 and minimize the performance index $J = \boldsymbol{x_0}^T P_d \boldsymbol{x_0}$, where $X_0 = \boldsymbol{x_0}\boldsymbol{x_0}^T$ is the matrix associated with the initial conditions.

$$r_i F_i C_i X C_i^T + B_i^T P_d X C_i^T = 0 \qquad \forall i = 1, 2 \tag{37}$$

$$A_0 X + X A_0^T + X_0 = 0 \tag{38}$$

$$A_0^T P_d + P_d A_0 + Q + \sum_{i=0}^{2} C_i^T F_i^T r_i F_i C_i = 0 \tag{39}$$

In [12] it was shown that such equations are necessary for the solution of the decentralized problem and that they are interdependent conditions. Then, to determine the decentralized feedback gain matrix F_d^*, it is necessary to use an algorithm. It can be said that the LQRd case is simpler to implement than the LQRc due to the amount of null elements, however, the characterization of the gain matrix is more laborious.

3 Results

To compare the performances of the 8, 4 and 6 pole Magnetic Bearing models, simulations were performed submitting the systems to the control laws presented: centralized and decentralized LQR, varying the rotation speed ω and the base current i_0 to portray different operating scenarios.

To find the matrices of the system's dynamic model and the constants k_p and k_v, physical parameters of the Magnetic Bearing prototypes are used [8], together with the base current i_0.

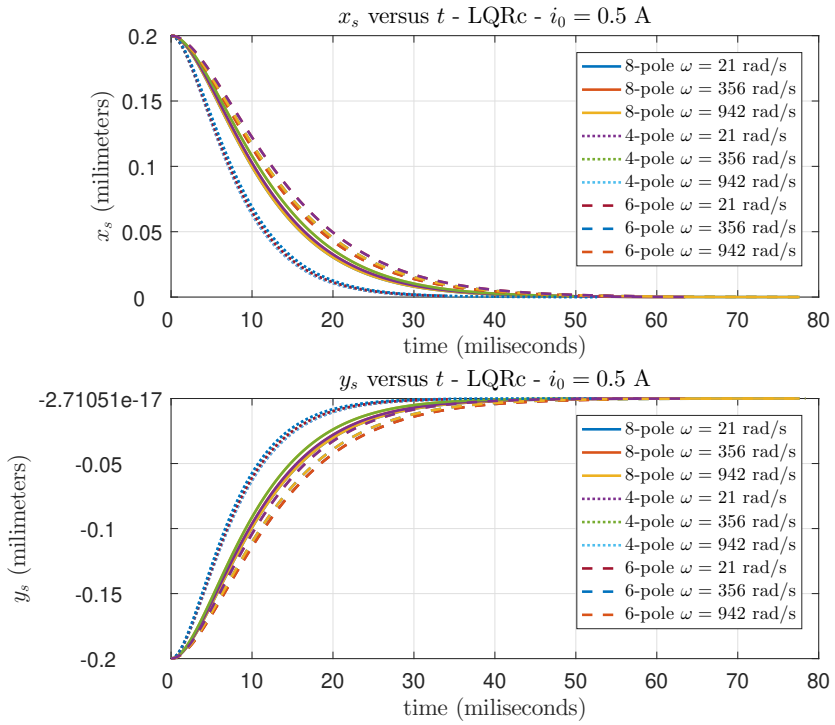

Figure 3: Centralized LQR response.

For the first set of simulations, the base current is considered $i_0 = 0.5$ A. The operating speeds ω used are 21 rad/s (approximately 200 rpm), 356 rad/s (approximately 3400 rpm) and 942 rad/s (approximately 9000 rpm). Figure 3 presents the LQRc response curves (x_s and y_s displacements) for each speed and geometry:

It is observed that the 4-pole bearing is the fastest to return to the equilibrium point, followed by the 8-pole and, lastly, the 6-pole bearing. The existing differences are small. It can also be noticed that the settling time increases as the operating speed increases. This fact suggests that lower operating speeds are better to stabilize the system. However, the variation in settling times for the 3 speeds used is much smaller for the 4-pole geometry than for the others.

Table 1: Closed loop eigenvalues - LQRc - $\omega = 356$ rad/s - $i_0 = 0.5$ A

Closed loop eigenvalues		
8 polos	**4 polos**	**6 polos**
$-191.9 \pm 5.74i$	$-285.7 \pm 6i$	$-167.7 \pm 5.58i$
$-149.4 \pm 4.47i$	$-200.7 \pm 4.22i$	$-128.1 \pm 4.26i$

In Table 1, the closed loop eigenvalues of the 3 geometries submitted to the operating speed

$\omega = 356$ rad/s can be observed. The real part of the eigenvalues in the 4-pole bearing is greater (in module) than the others, which confirms the shorter stabilization time indicated in the graph.

A simulation with the same scenario is carried out for the decentralized LQR control strategy, as shown in Figure 4:

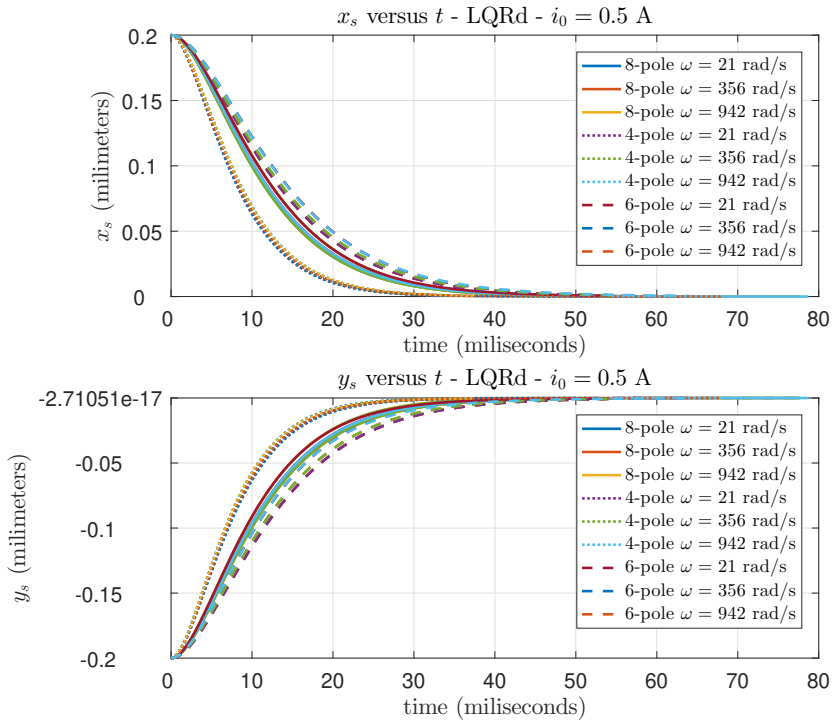

Figure 4: Decentralized LQR response.

The same characteristics found in the simulation of the LQRc control are observed, however, when comparing the two control strategies, the LQRd presents a minimal decrease in the real part of the eigenvalues, which generates a small increase in the stabilization time, as expected in this technique. Table 2 presents the closed loop eigenvalues:

Table 2: Closed loop eigenvalues - LQRd - $\omega = 356$ rad/s - $i_0 = 0.5$A

Closed loop eigenvalues		
8 polos	**4 polos**	**6 polos**
$-190.2 \pm 25.2i$	$-283.5 \pm 20.2i$	$-168 \pm 25.4i$
-133.9	-187.2	-115.1
-165	-216.4	-140

It can be stated that among the 3 compared geometries, the 4-pole one presents the best

performance, followed by the 8-pole and finally the 6-pole geometry. But still, the performances are quite similar.

Comparisons on the behavior of the system for the three speeds used (21 rad/s, 356 rad/s and 942 rad/s) were also carried out with the aim of analyzing whether such values can be defined as low, medium or high speed, as these values were determined based on previous works.

The procedure adopted was to compare the feedback matrices F and the closed-loop eigenvalues for the three rotation speeds ω. The centralized LQR feedback matrices for the 6-pole bearing and base current $i_0 = 0.5$ A are presented, respectively, in the equations 40 to 42:

$$F_c^{*6}\ (21\ \text{rad/s}) = \begin{bmatrix} -1168.9 & -2.1 & -8 & 0 \\ 2.4 & -1012.3 & 0 & -7 \end{bmatrix} \tag{40}$$

$$F_c^{*6}\ (356\ \text{rad/s}) = \begin{bmatrix} -1167.5 & -35.3 & -8 & 0 \\ 40.8 & -1011.1 & 0 & -7 \end{bmatrix} \tag{41}$$

$$F_c^{*6}\ (942\ \text{rad/s}) = \begin{bmatrix} -1159 & -93 & -8 & 0.1 \\ 107.4 & -1003.7 & 0.1 & -6.9 \end{bmatrix}. \tag{42}$$

The matrices have a similar structure. However, the elements f_{12} and f_{21} present a considerable difference, which suggests an impact promoted by the change in operating speed values. The eigenvalues for this situation are presented in table 3:

Table 3: Closed loop eigenvalues - LQRc - Six-pole MB - $i_0 = 0.5$ A

Closed loop eigenvalues		
21 rad/s	**356 rad/s**	**942 rad/s**
-166.27	$-167.76 \pm 5.58i$	$-167.26 \pm 15,29i$
-169.42	$-128.10 \pm 4.26i$	$-127.56 \pm 11.66i$
-129.39		
-126.98		

The eigenvalues present real part with very similar values, however, as the operating speed increases, the imaginary part also increases (in module), which generates a considerable impact on the oscillation frequency of the system response.

Therefore, with the significant changes observed in some elements of the feedback matrices and in the closed-loop eigenvalues of the system with the increase in the operating speed, we can consider the values used in this work - 21 rad/s (approximately 200 rpm), 356 rad/s (approximately 3400 rpm) and 942 rad/s (approximately 9000 rpm) - as low, medium and high speeds, respectively.

Another interesting study to be carried out is to understand how an optimal control law designed for a 6-pole magnetic bearing operating in a given angular speed range ω behaves when applied to other values of rotational speed.

The comparison was made considering the base current $i_0 = 1.5$ A and the centralized LQR control strategy. The optimal control law designed for the six-pole bearing operating at low speed, $\omega = 21$ rad/s, was applied in the mathematical models of low, medium ($\omega = 356$ rad/s) and high ($\omega = 942$ rad/s) speed. Figure 5 shows the response curves x_s and y_s for the three mathematical models:

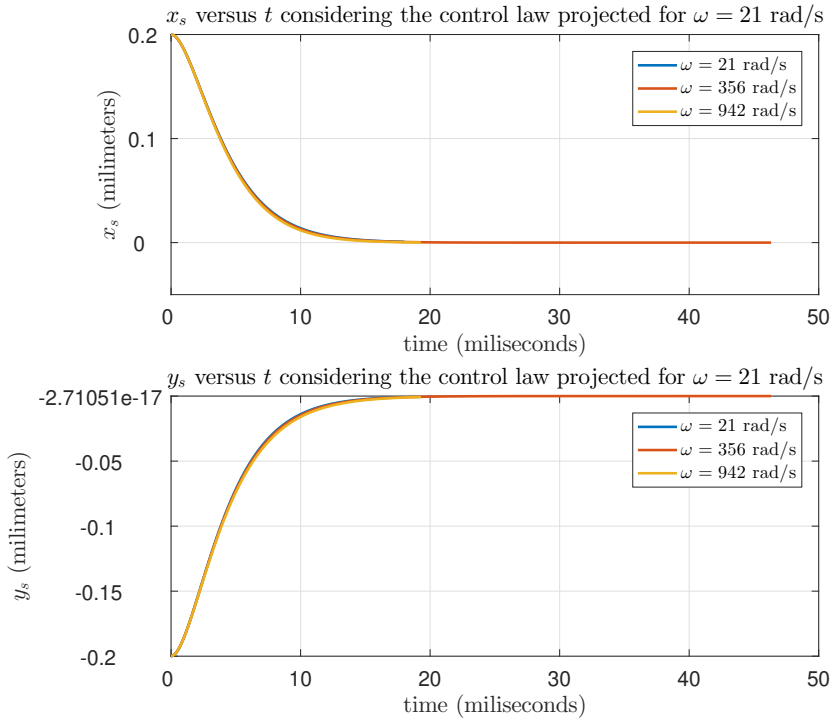

Figure 5: Comparison on the control law for low rotation speed $\omega = 21$ rad/s.

As can be seen, the three models behave well when subjected to a low speed control law, with no large discrepancy between the response curves. It can be said then that the system responds satisfactorily and very similarly when it operates at a rotation speed different from which the control law was designed.

4 Conclusions

The linear dynamic model of the 6-pole magnetic bearing was developed and shown in state space structure, presenting the decoupling characteristic between the control variables. Simulations to compare the three geometries were performed for two control strategies (centralized LQR and decentralized LQR) varying the values of the rotation speed ω.

It is concluded that the increase in rotation speed implies a small increase in the stabilization time necessary for the bearing to return to the central position. As for the results of the six-pole geometry presented, it was found that it had a slightly slower response time than the eight- and four-pole bearings.

In addition to comparing the existing geometries, a comparison was made between the rotation speeds used in this work and it was possible to define three operating speed ranges: low, medium and high. It was also studied the behavior of the system when applying a control law designed for a given rotation speed in the system operating at different speed, from which it was concluded that the system responds satisfactorily.

References

[1] V. R. Vasco, "Modelagem e controle ótimo de um mancal magnético de três polos," Master's thesis, UFRJ, 2019.

[2] H. BLEULER, *Decentralized control of magnetic rotor bearing systems*. PhD thesis, Swiss Federal Institute of Technology, 1984.

[3] W. Zhang and H. Zhu, "Radial magnetic bearings: An overview," *Results in Physics*, 2017.

[4] A. CHIBA, T. FUKAO, and e. ICHIKAWA, O., *Magnetic Bearings and Bearingless Drives*. Newnes-Elsevier, 2005.

[5] G. SCHWEITZER, H. BLEULER, and e. TRAXLER, A., *Magnetic Bearings*. vdf Hochschulverlag, 1994.

[6] G. Schweitzer, "Active magnetic bearings - chances and limitations," *6th International Conference on Rotor Dynamics*, 2002.

[7] D. F. B. DAVID, J. A. SANTISTEBAN, and A. C. D. N. GOMES, "Modeling and testing strategies for an interconnected four-pole magnetic bearing," *Actuators*, vol. 6, no. 3, 2017.

[8] P. H. S. PINTO, "Comparações teóricas e práticas sobre geometrias de mancais magnéticos," Master's thesis, COPPE, Universidade Federal do Rio de Janeiro, 2018.

[9] S. CHEN and C. HSU, "Optimal design of a three-pole active magnetic bearing," *IEEE Transactions on Magnetics*, vol. 38, no. 5, p. 3, 2002.

[10] R. M. Stephan, F. C. Pinto, A. C. D. Gomes, J. A. Santisteban, and A. O. Salazar, *Mancais Magnéticos - Mecatrônica sem atrito*. Editora Ciência Moderna Ltda., 1 edição ed., 2013.

[11] K. Ogata, *Engenharia de Controle Moderno*. Pearson, 2011.

[12] L. S. RODRIGUES, "Controle ótimo descentralizado a dois darâmetros para mancais-motores magnéticos," Master's thesis, COPPE, Universidade Federal do Rio de Janeiro, 2005.